



## OPEN Oyster recruitment and growth increases wave attenuation by breakwaters

Georgette L. Tso<sup>1</sup>✉, Siddharth Narayan<sup>1,3</sup>, Megan E. Geesin<sup>1</sup>, Hannah Sirianni<sup>2</sup>, Matthew A. Reidenbach<sup>4</sup>, Jens Figlus<sup>5</sup> & Rachel K. Gittman<sup>3,6</sup>

Coastal protection structures that incorporate reef-building organisms, such as oysters, are increasingly used to reduce wave energy, while also enhancing ecological function. However, it remains unclear how recruitment and growth of living organisms alters wave attenuation, and ultimately coastal protection, over time. Here, we present the first field-based quantification of changes in wave transformation over a living oyster breakwater following two seasons of recruitment. Using wave gauge deployments and oyster surveys at two sites, we observed a 10–15% increase in wave attenuation after oyster recruitment. The increase in wave attenuation was associated with oyster-induced increases in surface roughness and reductions in structural porosity. A standard breakwater transmission model was adapted using fitted ecological parameters, and oyster length emerged as an informative predictor of effective structural diameter. Our results highlight how ecological dynamics shape the evolving performance of nature-based coastal defenses and demonstrate a path toward adaptive, hybrid design frameworks.

Coastal hazards, including storm surge, flooding, erosion, and loss of land, present significant risks to human populations and infrastructure. As coastal populations and the concentration of critical infrastructure continue to grow, their vulnerability to hazards is exacerbated<sup>1</sup>. Without adaptation, sea level rise could expose hundreds of millions to flooding by 2100<sup>2</sup>. The need for coastal protection measures has become more urgent as hazards threaten ecosystems, economies, and settlements worldwide<sup>3,4</sup>.

Engineered structures such as bulkheads and seawalls are the most common method of protecting shorelines against wave and surge hazards but often have detrimental effects on natural ecosystems and processes<sup>5–8</sup>. With over 50% of coastlines already hardened in global urban centers<sup>9–11</sup>, there is a growing impetus for solutions that provide effective protection while harnessing the natural capacity of coastal habitats to attenuate waves and storm surges<sup>3,12,13</sup>. However, unlike static engineered structures, the coastal protection functions of nature-based adaptation strategies can change over time as their natural features evolve and change in size, shape, and form<sup>14</sup>.

Living breakwaters, also referred to as artificial reefs or living shorelines, exemplify nature-based adaptations that offer coastal protection. They consist of a man-made base structure and subsequent recruitment of living organisms to the structure<sup>15,16</sup>. By integrating engineered structures with natural habitats, living breakwaters serve as a buffer against wave energy<sup>17–19</sup>, mitigating erosion and storm surge impacts<sup>20,21</sup> while conserving and restoring reef ecosystems like coral<sup>22</sup>, oyster<sup>23–25</sup>, or mussel<sup>26</sup> reefs. Unlike traditional hard-engineering solutions, living breakwaters have the potential to adapt to dynamic environmental conditions, enabling self-repair and growth in response to sea-level rise and storm damage<sup>27,28</sup>. Their dual functionality—enhancing coastal resilience and providing critical ecosystem services<sup>8,29</sup>—positions living breakwaters as a promising alternative to purely static defenses, particularly in regions facing rising sea levels and intensifying hazards.

Reef-building organisms such as corals<sup>30</sup>, mussels<sup>31</sup>, and oysters are increasingly used in living breakwaters. Among these, oysters are especially widespread in restoration efforts, with oyster breakwaters implemented across diverse global settings— including the Gulf Coast and New York Harbor of the United States<sup>17,32</sup>, the Wadden Sea of the Netherlands<sup>33</sup>, the Bay of Bengal in Bangladesh<sup>20</sup>, and the Bohai Sea of China<sup>34</sup>. As an ecosystem engineer, oysters form three-dimensional, structurally complex, biogenic reefs that modify sediment

<sup>1</sup>Department of Coastal Studies, Integrated Coastal Programs, East Carolina University, Greenville, NC 27858, USA.

<sup>2</sup>Department of Earth, Environment & Planning, East Carolina University, Greenville, NC 27858, USA. <sup>3</sup>Coastal Studies Institute, East Carolina University, Wanchese, NC 27981, USA. <sup>4</sup>Department of Environmental Sciences, University of Virginia, Charlottesville, VA 22904, USA. <sup>5</sup>Department of Ocean Engineering, Texas A&M University, Galveston, TX 77554, USA. <sup>6</sup>Department of Biology, East Carolina University, Greenville, NC 27858, USA. ✉email: tsog21@students.ecu.edu

and wave dynamics<sup>20,35–37</sup>, thus providing nursery habitat and refuge for many marine species<sup>8,38</sup>. If conditions such as larval supply and exposure duration are suitable, oysters can colonize and form living reefs that accrete vertically at rates sufficient to keep pace with current, and potentially even accelerated, sea-level rise, making them self-sustaining elements of coastal protection<sup>27,28</sup>. However, a critical gap remains in understanding how long-term wave attenuation dynamics of oyster breakwaters are altered by biological recruitment<sup>39</sup>.

As oysters begin to colonize a breakwater and form a living reef, they induce structural changes: the surface becomes rougher as sharp oysters grow vertically<sup>27,36,40–44</sup>, structural porosity is reduced as oysters fill in interstitial spaces<sup>45</sup>, and crest height may increase through vertical accretion<sup>27–29</sup>. While structural changes from oyster colonization are expected to enhance wave attenuation, the specific effects of oyster recruitment and growth on overall reef performance remain poorly understood<sup>39</sup>. Most existing studies use bare structures in laboratory wave tanks<sup>46–48</sup> or assess field performance shortly after installation, before substantial oyster recruitment occurs<sup>17,49–51</sup>. Consequently, few studies capture how wave attenuation evolves with ecological succession<sup>39,43,52,53</sup>.

Standard engineering formulae that describe wave transformation over breakwaters do not account for the evolution of the breakwater structure as oysters recruit and grow. While these formulae have been successfully applied to bare oyster breakwaters<sup>46,54</sup>—they do not incorporate the dynamic, living aspects of reef development. Commonly used expressions, such as those by Numata (1975) and Tanaka (1976), translated in Goda and Ahrens<sup>55</sup>, were derived for low-crested rubble-mound breakwaters, where structure profiles remain fixed over time:

$$K_{T\text{ thru}} = \frac{1.0}{\left(1.0 + 1.135 \left(\frac{B_{eff, thru}}{D_{eff, thru}}\right)^{0.65} \left(\frac{H_I}{L}\right)^{0.5}\right)^2} \quad (1)$$

$$K_{T\text{ over}} = \max\{0, (1 - \exp[a(F/H_I - F_0)])\}, \text{ where} \\ a = 0.248 \exp[-0.384 \ln(B_{eff, over}/L_0)] \text{ and} \\ F_0 = \begin{cases} 1.0, & D_{eff, over} = 0 \\ \max\{0.5, \min(1.0, H_I/D_{eff, over})\}, & D_{eff, over} > 0 \end{cases} \quad (2)$$

Equation (1) predicts transmission *through* an emergent structure ( $K_{T\text{ thru}}$ ), where  $B_{eff}$  is the effective structure width,  $D_{eff}$  is the effective rubble or rock diameter,  $H_I$  is the incident wave height, and  $L$  is the wavelength. The ratio  $B_{eff}/D_{eff}$  characterizes the relative geometry and porosity of the structure, while  $H_I/L$  represents the wave steepness. Equation (2) predicts transmission over a submerged structure ( $K_{T\text{ over}}$ ), where  $F/H_I$  is the relative freeboard, the vertical distance between the still water level and the structure crest, normalized by the incident wave height  $H_I$ , the coefficient  $a$  is a shape parameter that scales with relative structure width  $B_{eff}/L$ , and  $F_0$  is the critical relative freeboard, which is dependent on  $H_I/D_{eff}$ .

Existing wave transmission models do not explicitly incorporate ecological processes such as oyster recruitment, but they rely on physical parameters—such as surface roughness, porosity, and crest elevation—that can be influenced by biological growth. As oysters colonize and modify reef structure, these parameters shift in ways that may significantly alter wave attenuation. While wave transmission models typically assume static structure geometry, the biological condition of the structure at the time of model input can still influence accuracy. Treating biologically altered structures as static, but updated, in form allows these ecological effects to be incorporated, even if ongoing growth is not explicitly simulated. Failing to account for these biologically mediated changes risks underestimating the wave attenuation capacity of living breakwaters and limits the development of ecologically responsive design guidance.

Drawing from knowledge on traditional low-crested breakwaters, the dominant modes of wave transmission can be separated into three zones based on relative freeboard  $F/H_I$  (Fig. 1a; black circles indicating Zones 1–3, Supplementary Fig. 1)<sup>56</sup>. In **Zone 1** ( $F/H_I < 0$ ), the structure is fully submerged and most wave energy is dissipated through bottom friction. In **Zone 2** ( $0 < F/H_I < 1$ ), the crest is partially exposed, and wave transmission occurs primarily via overtopping and runup. In **Zone 3** ( $F/H_I > 1$ ), the structure is emergent, overtopping is minimal, and wave energy is mainly transmitted through the pore spaces between artificial reef units (Fig. 1a)<sup>55,56</sup>.

Before colonization, oyster breakwaters function similarly to traditional low-crested breakwaters by design, attenuating waves while allowing a degree of wave overtopping and transmission to support sediment transport and ecological connectivity<sup>20,55,56</sup>. Once living organisms begin to recruit onto reef structures, however, their effects on wave transmission remain unclear. Given that reef-building organisms like oysters increase surface roughness, reduce porosity by infilling interstitial spaces, and raise crest elevation through vertical growth<sup>36,41,45</sup>, we hypothesized that ecological recruitment would reduce wave transmission across all relative freeboard zones. Specifically, we expected colonization to enhance frictional dissipation in Zones 1 and 2, limit runup and overtopping in Zone 2, and decrease transmission through the structure in Zone 3 (Fig. 1a).

Here, we present the first investigation of changes in wave transmission by oyster breakwaters as a function of oyster recruitment. We focus on modular concrete-based breakwaters colonized by *Crassostrea virginica*, the Eastern oyster, and develop relationships to model wave transformation over these dynamic structures. This work is based on field observations of two constructed oyster breakwaters in coastal North Carolina, United

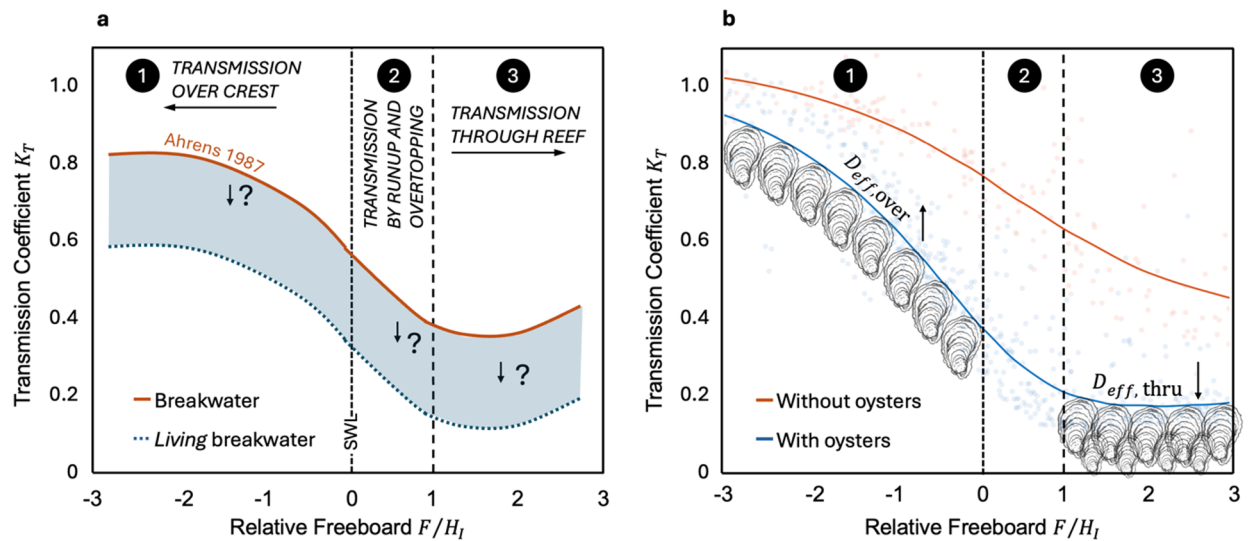


**Fig. 1.** Oyster recruitment alters wave transmission by modifying key structural parameters of breakwaters, with zone-specific effects linked to relative freeboard  $F/H_I$ . (a) Conceptual diagram demonstrating the three dominant modes of wave transmission as a function of relative freeboard for breakwaters, adapted from Ahrens' diagram for low-crested breakwaters<sup>56</sup>. Wave transmission is represented by the transmission coefficient,  $K_T$ , defined as a ratio of the transmitted wave height to the incident wave height. Relative freeboard is defined as the ratio of freeboard,  $F$ , the distance between the crest to the instantaneous water level, to  $H_I$ , the incident wave height. We hypothesize that oyster recruitment will reduce wave transmission across all relative freeboard zones. (b) Observed wave transmission decreased across all zones following oyster recruitment. The greatest reductions in wave transmission occurred in Zone 3, followed by Zones 2 and 1. These reductions were associated with oyster-induced changes to breakwater structure—such as increased surface roughness (linked to  $D_{eff, over}$ ) and decreased porosity (linked to  $D_{eff, thru}$ )—which modulate wave transformation differently across tidal zones.

States, measured immediately after construction and again after two seasons of oyster recruitment (Fig. 2). Specifically, we (1) investigate changes in wave attenuation by the breakwaters before and after successful oyster recruitment, (2) evaluate how recruitment alters the relationship between wave transmission and relative freeboard, and (3) adapt a standard transmission model for low-crested breakwaters by incorporating an effective diameter parameter that accounts for biological growth. Our findings represent a first step toward quantifying wave transformation over living, ecologically dynamic breakwater structures by integrating empirical wave transmission models with field-measurable ecological parameters.

## Results

### Oyster recruitment

#### Reef surfaces

At both sites, oyster density and length generally increased toward the lower half of the structures, consistent with longer submersion favoring settlement<sup>57</sup>. This elevation gradient was especially pronounced at Site 1, where the upper half remained largely bare while dense colonies of larger oysters occupied the lower half (Figs. 3 and 4c and f; Supplementary Tables 3 and 4). At Site 2, oysters colonized both halves, though a vertical gradient was still apparent. Despite these trends, only oyster length, not density, differed significantly with elevation: oysters on the lower half were significantly longer than those on the upper half at both sites (Site 1:  $5.9 \pm 1.3$  cm,  $n = 35$  vs.  $3.2 \pm 2.1$  cm,  $n = 35$ ;  $p = 4.4 \times 10^{-5}$ ; Site 2:  $4.6 \pm 1.5$  cm,  $n = 60$  vs.  $2.5 \pm 1.4$  cm,  $n = 60$ ;  $p = 1.2 \times 10^{-6}$ ; Supplementary Tables 3 and 4). Oysters on the seaward side also tended to be denser and longer than those on the landward side at both sites, though again, only differences in oyster length were statistically significant (Site 1:  $n = 35$ ,  $p = 0.041$ ; Site 2:  $n = 60$ ,  $p = 0.022$ ; Supplementary Tables 3 and 4).

Importantly, oyster length also varied between sites when considering the elevation gradient and seaward faces. On the seaward face, oysters were significantly longer at Site 1 than Site 2 ( $5.0 \pm 1.6$  cm,  $n = 20$  vs.  $4.2 \pm 1.8$  cm,  $n = 30$ ;  $p = 0.02$ ; Supplementary Table 3). A similar trend was observed for oysters on the lower half of the breakwaters, where oysters at Site 1 ( $5.9 \pm 1.3$  cm,  $n = 15$ ) were significantly longer than those at Site 2 ( $4.6 \pm 1.5$  cm,  $n = 30$ ;  $p = 0.0057$ ; Supplementary Table 3). No significant differences in oyster density were detected between sites for either the seaward face or lower half.

#### Reef gaps

By June 2024, live oysters had partially infilled and cemented the gaps between breakwater units, with mean gap coverage reaching  $80 \pm 26\%$  at Site 1 ( $n = 6$ ) and  $25 \pm 22\%$  at Site 2 ( $n = 6$ ;  $p = 0.054$ ; Figs. 3 and 4c and f; Supplementary Table 2). Within these gaps, oysters at Site 1 were significantly longer than those at Site 2

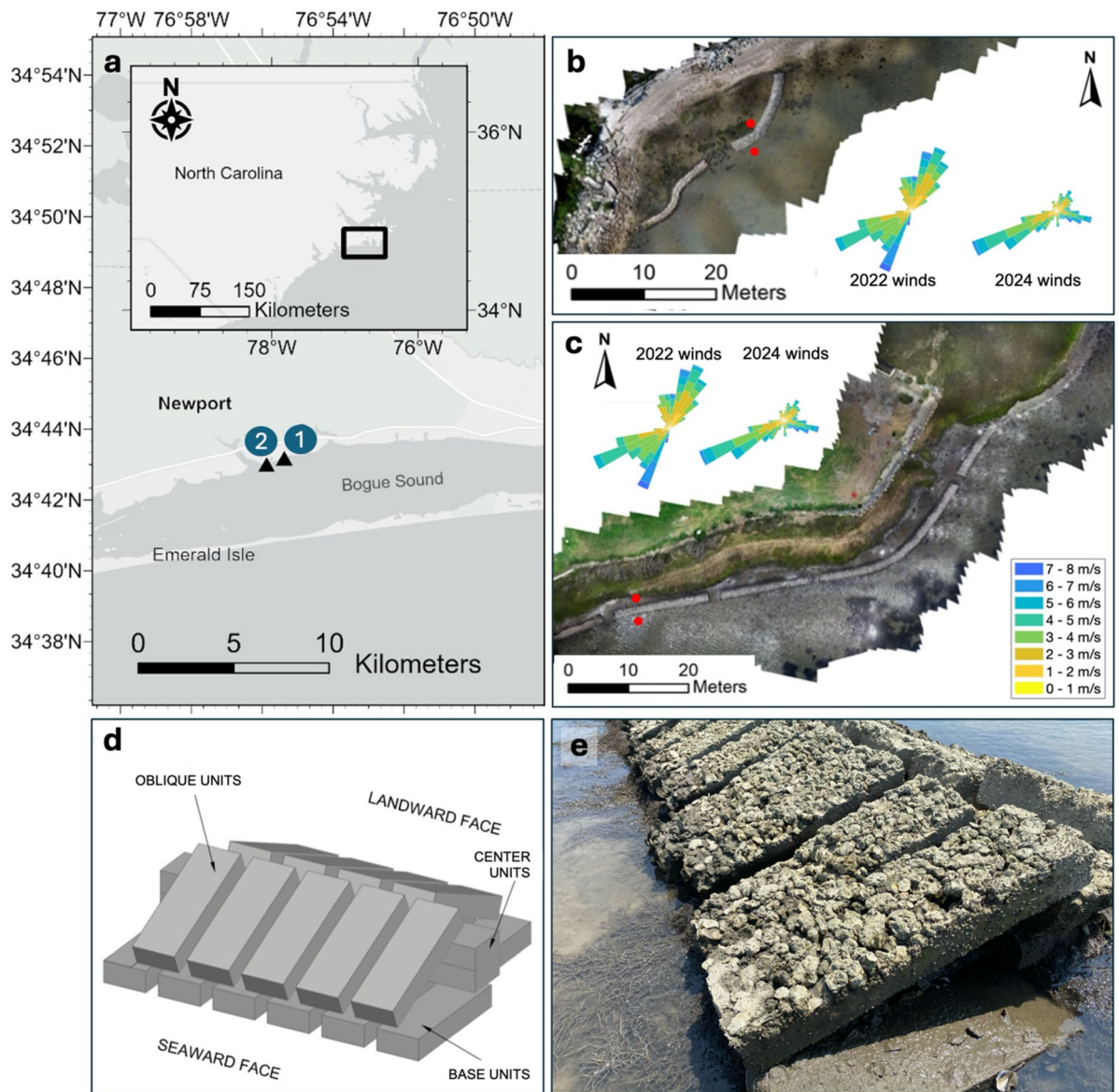


**Fig. 2.** Study site locations and structural configurations of the deployed oyster breakwaters in Newport, North Carolina, USA. **(a)** Map showing study site locations. Sites 1 (34.7203° N, 76.9381° W) and 2 (34.7284° N, 76.9482° W) are marked. **(b, c)** Orthomosaics of Site 1 and Site 2 QuickReef structures, respectively. Red dots indicate wave gauge locations. Wind roses from Beaufort (NDBC Station ID: BFTN7), ~ 20 km east of both sites, are overlaid. **(d)** Orthogonal view of a section of a QuickReef breakwater. Crest height and base width are approximately 0.60 m and 1.60 m respectively. Oblique and base unit slabs are approximately 0.80 × 0.25 × 0.15 m while the two stacked center units are approximately 0.80 × 0.15 × 0.15 m. Slope is approximately 3:4 (vertical: horizontal). Intentional gaps between adjacent base and oblique units are left to facilitate oyster larval recruitment, attachment, and growth. While gap widths vary slightly due to manual construction (0.01–0.07 m), there were no significant differences between sites. Drawing from Native Shorelines, not to scale. **(e)** QuickReef structure immediately post-construction at Site 2.

( $5.3 \pm 1.0$  cm,  $n = 15$  vs.  $4.2 \pm 0.8$  cm,  $n = 15$ ;  $p = 0.0027$ ; Supplementary Table 2). A vertical gradient in oyster density was also present in the gaps: at Site 1, coverage increased from  $70 \pm 26\%$  at the top ( $n = 3$ ) to  $90 \pm 10\%$  at the bottom ( $n = 3$ ). At Site 2, oysters favored the surface over the gaps, with 0% coverage at the top ( $n = 3$ ) and only  $40 \pm 43\%$  at the bottom ( $n = 3$ ; Supplementary Table 3).

### Wave transmission

Wave transmission decreased across all zones and both sites following oyster recruitment. Tidal conditions and incident wave heights were comparable between sites during both the 2022 and 2024 deployments, though incident wave heights were slightly higher in 2024 (Supplementary Table 1). In 2022, the Site 1 breakwater

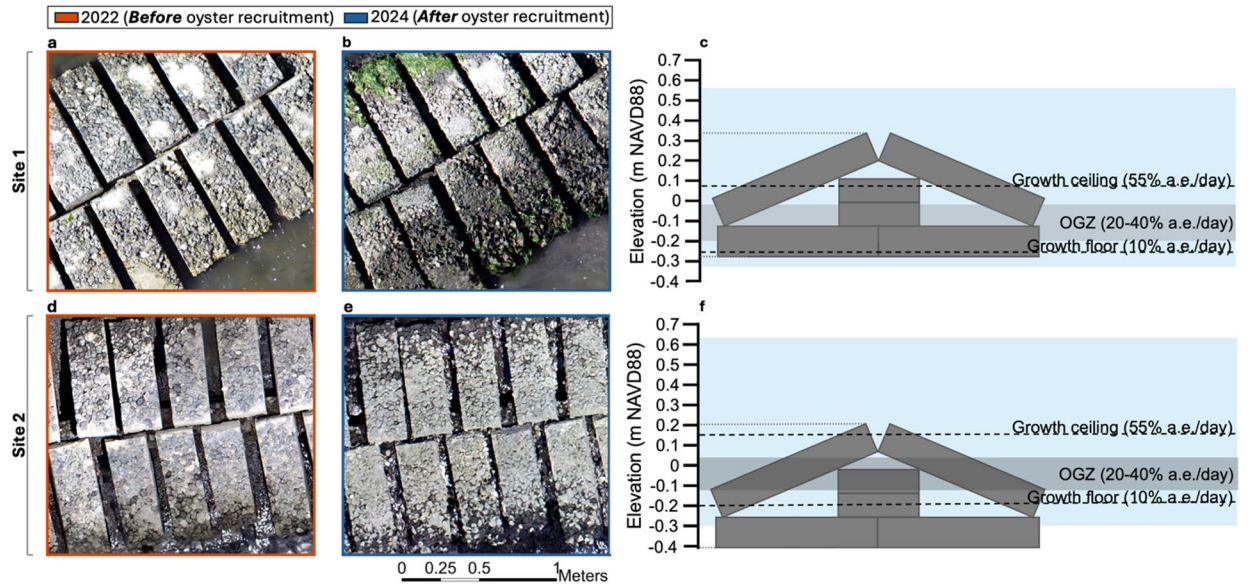


**Fig. 3.** Oyster recruitment to reef surfaces and gaps differed between Sites 1 and 2. Photos show surfaces and gaps at Sites 1 (a, b) and 2 (d, e) before (2022) and after (2024) oyster recruitment. Site 1 supported significantly longer oysters than Site 2 on seaward and lower half of structure surfaces. In reef gaps, Site 1 supported greater oyster coverage and larger individuals than Site 2. Cross-sectional diagrams (c, f) illustrate elevation differences between breakwaters. Site 2 was constructed at a lower elevation, placing more of its surface within the Optimal Growth Zone (OGZ), defined as the tidal window experiencing 20–40% aerial exposure (a.e.) per day, where *Crassostrea virginica* achieves maximum growth<sup>28</sup>. Growth declines above the growth ceiling (55% a.e./day) and below the growth floor (10% a.e./day)<sup>28</sup>.

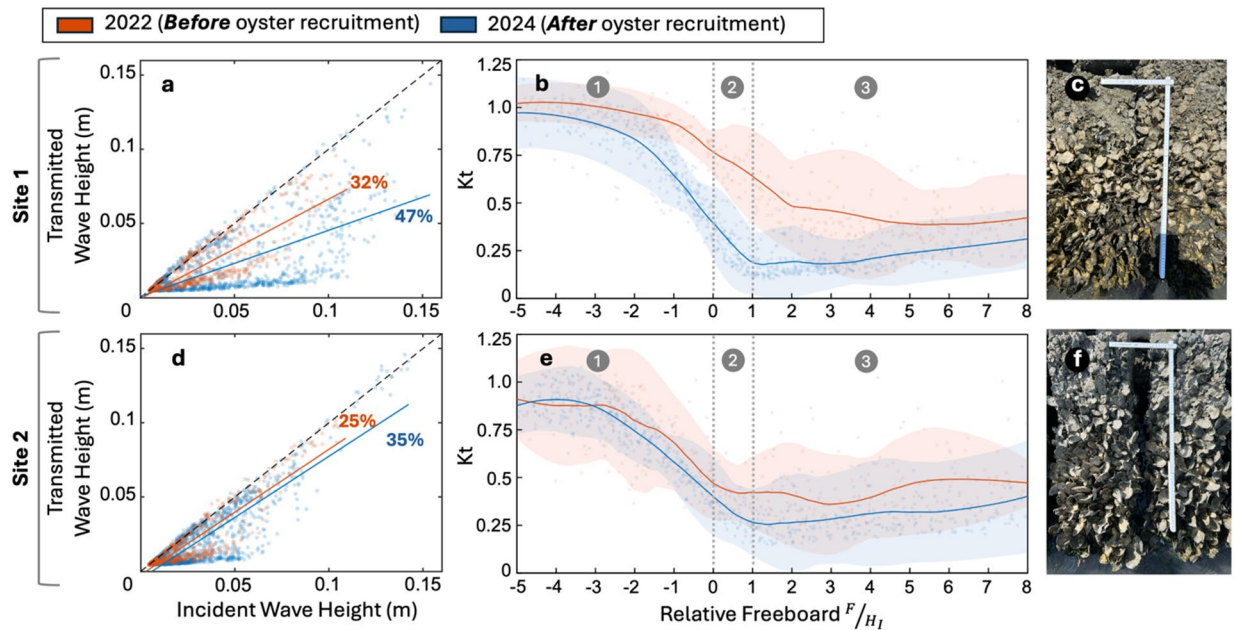


**Fig. 4.** Oyster recruitment reduces wave transmission across all relative freeboard zones. (a, d) Transmitted vs. incident wave heights for Sites 1 and 2, before (2022, orange) and after (2024, blue) oyster recruitment. Shaded points represent significant wave heights; solid lines are linear regressions; the dashed black line indicates 1:1 transmission. (b, e) Wave transmission coefficients ( $K_t$ ) as a function of relative freeboard ( $F/H_1$ ), with Locally Estimated Scatterplot Smoothing (LOESS) regression curves and shaded 95% confidence intervals. Vertical zones indicate submerged (1), partially emergent (2), and fully emergent (3) conditions. (c, f) Photos of artificial reef units in 2024 at Sites 1 and 2, showing differences in oyster cover following recruitment.

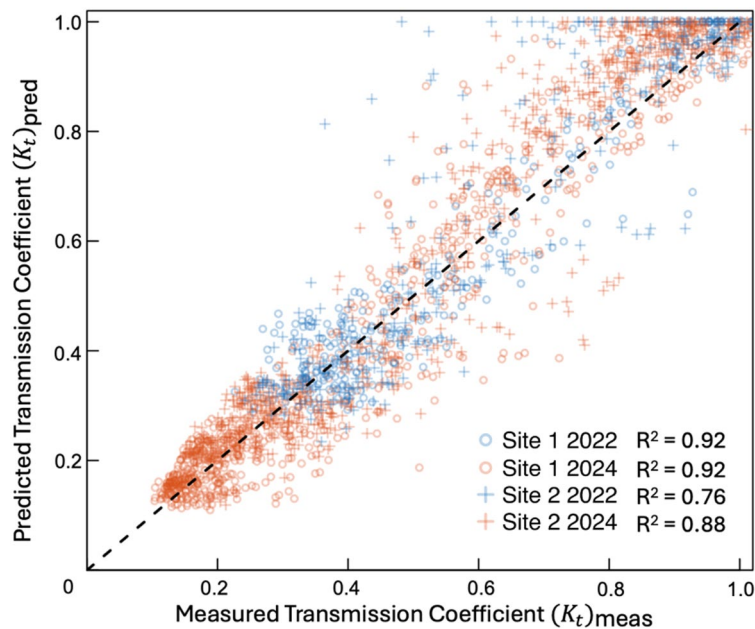


**Fig. 5.** Comparison of predicted and measured wave transmission coefficients. Measured coefficients ( $K_{T,meas}$ ) are defined as the ratio of transmitted to incident wave height. Predicted values ( $K_{T,pred}$ ) were calculated using the Goda and Ahrens (2008) model with fitted effective width parameters. The dashed line represents perfect agreement ( $K_{T,meas} = K_{T,pred}$ ).  $R^2$  values reflect model performance across sites and years.

Dataset	$n$	Mean	Standard deviation
Site 1 2024	962	0.0024	0.079
Site 1 2022	304	0.0060	0.070
Site 2 2024	707	0.0303	0.092
Site 2 2022	270	0.0279	0.120

**Table 1.** Sample size ( $n$ ), mean, and standard deviation of model residuals ( $\Delta K_T = K_{T,pred} - K_{T,meas}$ ) for each site and year.

attenuated 32% ( $\pm 28\%$ ) of incoming wave energy, while Site 2 attenuated 25% ( $\pm 25\%$ ). By 2024, attenuation increased to 47% ( $\pm 35\%$ ) and 35% ( $\pm 25\%$ ) at Sites 1 and 2, respectively (mean  $\pm$  standard deviation; Fig. 4a,d).

Reductions in wave transmission coefficients ( $K_i$ ) were observed across all three relative freeboard zones (Fig. 4b,e; Supplementary Table 6). In Zone 1 (submerged conditions),  $K_i$  decreased from 0.89 to 0.73 at Site 1 ( $-18\%$ ), and from 0.83 to 0.79 at Site 2 ( $-5\%$ ). In Zone 2 (partially emergent conditions),  $K_i$  decreased from 0.57 to 0.30 at Site 1 ( $-47\%$ ) and from 0.47 to 0.39 at Site 2 ( $-18\%$ ). In Zone 3 (emergent conditions),  $K_i$  decreased from 0.41 to 0.21 at Site 1 ( $-49\%$ ) and from 0.42 to 0.30 at Site 2 ( $-28\%$ ).

### Applicability of Goda and Ahrens (2008) breakwater transmission model to wave transformation over a growing oyster breakwater

The Goda and Ahrens (2008) breakwater transmission model accurately predicted wave transmission over oyster reef structures when effective width parameters ( $D_{eff,over}$  and  $D_{eff,thru}$ ) were calibrated via iterative parameter optimization to maximize model fit (Fig. 5; Table 1; Supplementary Fig. 2). The agreement between predicted and measured transmission coefficients was strong, with coefficients of determination ( $R^2$ ) ranging from 0.76 to 0.92 across sites and years: 0.92 for Site 1 (2022), 0.92 for Site 1 (2024), 0.76 for Site 2 (2022), and 0.88 for Site 2 (2024).

Mean error ( $\Delta K_T = K_{T,pred} - K_{T,meas}$ ) was low in all cases, though a tendency toward slight over-prediction of transmission coefficient  $K_T$  was observed (Table 1).

### Linking effective diameter $D_{eff}$ to oyster length

We evaluated how mean oyster length influences  $D_{eff,over}$  and  $D_{eff,thru}$  using Bayesian linear regression. The model for  $D_{eff,over}$  showed a positive association with oyster length (posterior mean slope  $\beta_1 = 0.0511$ , 95% CI: [0.003, 0.099]), with a 97.8% probability that the effect is positive. While the credible interval included

zero, the posterior suggests that larger oysters reduce overtopping by increasing roughness and crest elevation (Supplementary Fig. 3).

In contrast, the model for  $D_{eff, thru}$  showed a weak negative trend with oyster length ( $\beta_1 = -0.0150$ , 95% CI:  $[-0.033, 0.003]$ ), with a 96.5% probability of a negative effect. This suggests that larger oysters reduce porosity by filling interstitial spaces within the reef structure, although residual uncertainty remains high.

Other predictors (e.g., percent gap coverage) were also tested but showed no strong effects; results are reported in Supplementary Tables 8 and 9.

## Discussion

Our study provides the first field-based quantification of changes in wave transformation over a living oyster breakwater as it evolves through oyster recruitment and growth and introduces an empirical approach to estimate this transformation using a standard coastal engineering formula and field-measurable metrics such as oyster length. While previous studies on oyster breakwaters have focused on their ecological or hydrodynamic functions independently<sup>39</sup>, this study bridges those domains by linking biological recruitment to quantifiable changes in wave attenuation performance. Across all three relative freeboard zones, we observed that wave attenuation increased following oyster recruitment, with the greatest reductions in wave transmission occurring in Zone 3 (emergent conditions<sup>56</sup>, followed by Zones 2 and 1 (Figs. 1b and 4b and e; Supplementary Table 6). These results suggest that oyster-driven changes to breakwater structure—such as increased surface roughness and decreased porosity—have zone-specific impacts on wave transformation. Moreover, we found that mean oyster length was an informative predictor of these changes, offering a promising ecological indicator for forecasting the performance of living breakwaters over time.

Changes in wave attenuation varied between the two sites and across relative freeboard zones, highlighting the zone-specific impacts of oyster recruitment on wave-structure interactions. In Zone 1, where oyster breakwaters are fully submerged and wave energy is primarily dissipated through bottom friction, Site 1 exhibited an 18% reduction in wave transmission after recruitment, compared to only a 5% reduction at Site 2 (Fig. 4b,e; Supplementary Table 6). This difference is likely attributable to the larger oysters at Site 1 (Supplementary Table 3), which enhanced surface roughness and increased frictional resistance. In Zone 3, where emergent structures primarily dissipate wave energy through wave breaking and porous flow, both sites showed substantial reductions in transmission— Site 1 with a 49% reduction and Site 2 with 28% (Fig. 1b,e; Supplementary Table 6). These reductions appear to be driven less by increased surface roughness and more by decreased porosity as oysters colonized gaps and internal voids. This was especially apparent at Site 2, where short yet abundant oysters reduced transmission under emergent conditions. Although we could not directly observe the internal breakwater core, the dense surface and gap colonization at both sites suggests similar recruitment within interstitial spaces, likely contributing to decreased permeability and increased attenuation. Together, these results emphasize that different structural mechanisms—frictional dissipation versus porosity-driven flow resistance—dominate in different tidal zones and are modulated by the spatial characteristics of oyster growth.

To quantify how biological recruitment alters breakwater-scale wave transformation, we applied the Goda and Ahrens<sup>55</sup> breakwater transmission model using optimized effective diameter parameters. The model performed well overall, with  $R^2$  values exceeding 0.75 across sites and years, and particularly strong agreement in Zone 3, where wave breaking and porosity dominate dissipation (Fig. 5; Table 1; Supplementary Fig. 2). Agreement was weaker in Zones 1 and 2, where a mix of processes—bottom friction, runup, and porous flow—create more complex wave-structure interactions. Additionally, data partitioning by zone reduced sample sizes, limiting statistical power (Supplementary Table 7). Still, the model successfully captured the direction and magnitude of changes in wave transmission, demonstrating its potential to represent biologically dynamic structures when parameterized appropriately. These results suggest that integrating ecological metrics into standard engineering frameworks offers a promising path toward modeling the evolving performance of living shorelines.

To further explore how ecological recruitment modifies structural parameters relevant to wave attenuation, we tested empirical relationships between oyster length and the effective diameter terms used in the Goda and Ahrens model. Mean surface and gap oyster length were associated with variation in both  $D_{eff, over}$  and  $D_{eff, thru}$ , supporting their role as biologically grounded proxies for structure evolution. In Zone 1, where overtopping dominates, longer oysters likely increased crest complexity and surface roughness, contributing to reductions in wave runup. This was reflected in a positive correlation between oyster length and  $D_{eff, over}$ , aligning with the formulation for the runup limit  $F_0$ . In Zone 3, where wave transmission occurs primarily through porous flow, we observed a negative correlation between oyster length and relative permeability  $\frac{D_{eff, thru}}{D_{eff, thru}}$ , consistent with the idea that larger oysters reduce internal porosity by infilling reef gaps. While these relationships are preliminary and based on a small sample size, they support the theoretical basis for incorporating ecological metrics—particularly oyster size—into predictive models of living shoreline performance.

The observed differences in oyster recruitment and growth between Site 1 and Site 2 were likely shaped by tidal submergence, structural elevation, and predator-prey dynamics<sup>28,57–62</sup>. Although both sites used identical breakwater units, Site 1's higher elevation limited recruitment to the lower half of the structure, likely due to increased aerial exposure and desiccation stress (Fig. 3)<sup>28</sup>. In contrast, Site 2, which remained submerged for longer periods, supported oyster colonization across the entire reef surface. However, these oysters were significantly shorter on seaward and lower surfaces, suggesting that greater submersion time may have increased larval settlement but also intensified competition for resources and exposure to aquatic predators<sup>57</sup>. Prolonged submersion at Site 2 may have allowed greater access for stone crabs and sheephead, both known oyster predators<sup>57</sup>, potentially suppressing oyster linear growth by diverting energy toward shell thickening as a defense response<sup>58</sup>. Meanwhile, the slightly higher wave energy at Site 1 may have limited access for smaller, less wave-tolerant predators such as mud crabs (Supplementary Table 1)<sup>59–61</sup>, potentially reducing predation pressure

between breakwater units and facilitating greater oyster recruitment in breakwater gaps (Supplementary Table 2)<sup>62</sup>. These localized ecological dynamics contributed to the differences in oyster morphology and distribution observed between the two sites, ultimately shaping the trajectory and magnitude of wave attenuation increases.

Several limitations should be acknowledged. First, our analysis was constrained to two sites over a two-year recruitment period, limiting our ability to evaluate long-term reef accretion dynamics or responses to episodic storm events. Secondly, reflected waves were not measured seaward of the breakwaters due to instrumentation constraints, meaning that estimated incident wave heights may include both incident and reflected components. As a result, the transmission coefficients reported here represent combined energy losses from transmission and reflection, and we cannot resolve their relative contributions. This is a critical limitation given that oyster recruitment, particularly to interstitial voids, may reduce porosity and enhance reflection, rather than increasing internal dissipation alone. Recent studies have shown that changes in pore pressure distribution within porous breakwaters, driven by internal wave damping, can significantly influence transmission and reflection behavior<sup>63</sup>. While we cannot rule out reflection as a key contributor to the observed attenuation, the breakwaters studied here were sloping, rough, and highly porous—characteristics known to minimize wave reflection under most field conditions<sup>64</sup>. Thirdly, the Goda and Ahrens<sup>55</sup> model used in this study incorporates wave breaking effects indirectly through empirical parameterization but does not resolve the location or mechanism of breaking. Although knowledge of wave breaking regimes allow us to qualitatively attribute energy losses to friction in Zone 1 and breaking and/or internal damping in Zone 3, our inability to resolve wave breaking in situ introduces additional uncertainty. Furthermore, while the Goda and Ahrens<sup>55</sup> model performs well for permeable, trapezoidal breakwaters such as the ones examined in this study, its empirical basis limits direct generalization to other morphologies. Although other models (Ahrens<sup>56</sup>, Tomasicchio and Alessandro<sup>80</sup>) were tested, they yielded less satisfactory fits for our dataset. The Ahrens<sup>56</sup> model, originally developed for homogenous reef-type structures with narrow crests, applies separate equations for submerged and emergent conditions, producing a discontinuity in predicted transmission near the transition between overtopping- and through-flow-dominated regimes. In contrast, the Tomasicchio and D'Alessandro<sup>80</sup> model, though based on a larger and more heterogeneous dataset including impermeable and composite structures, smooths out permeability-dependent trends, reducing its accuracy for the porous, trapezoidal geometries considered here. These differences highlight the need for further refinement and validation of transmission models across a wider range of hybrid reef shapes and material properties. Finally, the empirical relationships between oyster length and effective diameter parameters were derived from a small sample size and should be validated across more sites and broader environmental gradients. Additional surveys are planned to expand temporal coverage and improve the statistical robustness of relationships between effective diameter and oyster-reef development. Future datasets incorporating additional time points and sites will allow more rigorous testing of these trends. Despite these constraints, our approach demonstrates the feasibility of integrating ecological measurements into engineering frameworks. Expanding this work across temporal and spatial scales will be critical to refining models and supporting design guidance for adaptive, living shoreline systems.

Together, our findings demonstrate that oyster recruitment can measurably enhance the performance of breakwaters by reducing wave transmission through mechanisms tied to both surface roughness and structural porosity. These biologically driven changes are not uniform but vary across tidal zones and site conditions, underscoring the importance of context-specific design in nature-based coastal protection (Fig. 1b). For practitioners, our results suggest that incorporating an estimated 5–18% reduction in the wave transmission coefficient  $K_T$  (Kt), over time may be appropriate for similar structures with strong oyster recruitment potential, with reductions closer to 18% for structures supporting longer oysters (mean lengths > 5 cm) and closer to 5% for those with shorter oysters (< 5 cm). These values provide conservative benchmarks based on our field data and may be particularly relevant for systems with high recruitment potential, especially under emergent or intertidal conditions. While these reductions will vary with local hydrodynamics, structural design, and recruitment dynamics, integrating a dynamic Kt \:  $K_T$  parameter informed by ecological metrics can support more adaptive and resilient breakwater designs.

By demonstrating how ecological parameters can be incorporated into existing engineering frameworks, this study advances the development of adaptive design tools for nature-based infrastructure. As climate change accelerates sea-level rise and intensifies storm impacts, integrating biological feedbacks into coastal planning will be essential for building resilient, sustainable shorelines. Future research should expand on these relationships over longer timescales, exploring how continued reef development interacts with sea-level rise, storm regimes, and broader ecosystem functions.

## Methods

### Study sites

Two private waterfront properties in Carteret County, North Carolina, USA were selected as study sites. Both properties had novel concrete-based breakwater systems called QuickReef<sup>®</sup> installed between May – June 2022 (Fig. 2). Designed by Native Shorelines A Davey Company, QuickReef<sup>®</sup> is a sloped breakwater composed of stacked concrete slabs with intentional gaps between slabs to allow water flow and facilitate larval oyster recruitment (Fig. 2). Concrete material is enriched with calcium carbonate and limestone marl to further facilitate larval attachment and oyster growth.

Due to their proximity, Site 1 and Site 2 experience similar wind and wave conditions. While Bogue Sound is characterized by generally low wave energy, the ~4,500 m fetch in the direction of dominant summer winds (200°–250°) can produce wind-driven waves up to 0.2 m during non-storm conditions (Fig. 2). Water depth and tidal range were comparable between the two sites during both the 2022 and 2024 deployments (Supplementary Table 1).

### Oyster sampling and analysis

Oyster sampling was conducted in September 2023, following two full seasons of oyster recruitment after reef installation. At each site, 0.0625 m<sup>2</sup> quadrats were placed at the two ends and center of each QuickReef<sup>®</sup> structure, at the upper half and lower half of each structure ( $n = 12$  quadrats per structure), and oyster density was assessed through species identification, counts, and percent cover<sup>65</sup>. Within each quadrat, shell length measurements were recorded for five distinct randomly selected oysters<sup>66</sup> ( $n = 60$  lengths per structure). For quadrats without oysters, both density and length were recorded as zero. The choice to record oyster length as “zero” rather than “Not a Number NaN” when no oysters are present enabled the use of mean oyster length as a predictor, particularly for structures prior to recruitment, when linking biological parameters to effective diameter in the Goda and Ahrens<sup>55</sup> model. Quadrat elevations were surveyed using a Trimble R10 real-time kinematic global navigation satellite system (RTK-GNSS) receiver ( $\pm 8$  mm horizontal,  $\pm 15$  mm vertical)<sup>67</sup>. To ensure statistical comparisons of oyster recruitment between sites were based on equivalent tidal elevations, oyster quadrats from Site 1 that exceeded the maximum crest elevation at Site 2 were excluded from analysis (Site 1:  $n = 7$  quadrats,  $n = 35$  quadrats).

The seaward gaps between breakwater slabs were sampled in June 2024, with each inter-slab gap (upper half vs. lower half) treated as a separate quadrat ( $n = 6$  per structure, Fig. 2). Five random distinct oyster lengths were measured within each gap  $n = 15$  lengths per structure).

Oyster surface densities and lengths were grouped by site, structure face (seaward vs. landward), and vertical position (upper vs. lower half). For each group, mean values and standard deviations were calculated. Two-tailed Welch's  $t$ -tests were used to evaluate differences between group means, as this test does not assume equal variances and is robust to moderately non-normal distributions. For each comparison, we report the test statistic ( $t$ ), degrees of freedom ( $df$ ), 95% confidence intervals for the difference in means, and effect sizes (Cohen's  $d$ ), calculated as the difference in group means divided by the pooled standard deviation. Normality was not formally tested due to small sample sizes in some comparisons. No corrections were applied for multiple comparisons, as tests were used to explore general patterns rather than test predefined hypotheses. All results were interpreted cautiously.

### Wave observations and data processing

Arduino-based wave gauges<sup>68</sup> were deployed 1 m landward and seaward of the QuickReef<sup>®</sup> structures to measure wave attenuation across each structure. Wave gauges recorded pressure continuously at 10 Hz between August 9th – 15th, 2022 and June 5th – 15th, 2024. Wave frequency data were divided into overlapping 10-minute windows with 50% overlap ( $n = 844$  in 2022,  $n = 1440$  in 2024), and start and end times were trimmed to ensure identical window intervals across both sites. The height of each sensor above the sediment bed was recorded. Water depth was calibrated with a manual water depth measurement at the time of deployment. Visual inspection of time series was performed, and anomalies were removed.

Water depth ( $h$ ) was calculated by subtracting atmospheric pressure ( $p_{atm}$ ) data from the National Buoy Data Center (NBDC) Cape Lookout station (Station ID: CLKN7)<sup>69</sup> and by dividing by the product of brackish water density ( $\rho = 1025$  kg/m<sup>3</sup>) and gravitational acceleration ( $g$ ). Sensor height above bed ( $d_s$ ) was added to obtain final water depth.

$$h = \frac{p - p_{atm}}{\rho g} + d_s \quad (3)$$

To account for pressure attenuation with depth, frequency-dependent back-correction was performed. For a specified wave frequency, the pressure attenuation factor is<sup>70</sup>:

$$K_p = \frac{\cosh(kd_s)}{\cosh(kh)} \quad (4)$$

where  $k$  is the wavenumber, calculated from linear wave theory as:

$$\omega^2 = gk \tanh(kh) \quad (5)$$

The water surface elevation power spectral density  $S_{\eta\eta}$  was estimated from the dynamic pressure power spectral density  $S_{pp}$ :

$$S_{\eta\eta} = \frac{1}{K_p^2} \times \frac{S_{pp}}{\rho^2 g^2} \quad (6)$$

Significant wave height was calculated as:

$$H_{m0} = 4\sqrt{m_0} = 4\sqrt{\int_0^\infty S_{\eta\eta}(f) df} \quad (7)$$

The wave transmission coefficient was calculated as:

$$K_t = \frac{H_T}{H_I} \quad (8)$$

Where  $H_T$  and  $H_I$  are the transmitted and incident significant wave height, respectively. Wave transmission coefficients were derived from these continuous wave gauge data, and each 10-minute wave record was treated as an independent observation for statistical analysis. Reflected wave heights were not measured seaward of the breakwaters due to a limited number of available pressure transducers. As a result, the estimated incident wave height ( $H_I$ ) likely includes contributions from both incident and reflected waves. However, reflected components were assumed to be negligible relative to incident wave energy, given the sloping, porous, and rough nature of the structures (see Fig. 2)<sup>64</sup>. Across both sites and both years, the ratio of group velocities at the transmitted and incident gauges ( $c_{g,t}/c_{g,i}$ ) ranged from 0.90 to 1.02. This implies that shoaling is negligible and the difference between a flux-based transmission estimate and the height-based transmission coefficient is  $\leq 5\%$ . We therefore use  $K_t$  as an appropriate metric of wave transmission, while noting that it is directly comparable to existing low-crested breakwater formulations.

All pressure data were processed using MATLAB<sup>71</sup> and the Ocean Wave Analysis Toolbox OCEANLYZ<sup>72</sup>. Data were plotted using MATLAB<sup>71</sup> and R<sup>73</sup>, including the mSIR package<sup>74</sup>.

### sUAS imagery and elevation mapping

Small uncrewed aerial systems (sUAS) surveys were conducted using a DJI Phantom 4 Pro to map structural features of oyster breakwaters before and after ecological recruitment. Pre-recruitment flights were conducted on May 15, 2022 and June 22, 2022, and post-recruitment flights were conducted on May 4, 2023 and June 18, 2023 for sites 1 and 2, respectively. To increase the accuracy of the GNSS data collected in the field, a survey-grade benchmark was created in 2022 for each study site, and ground control points (GCPs) were surveyed using the Trimble Spectra Precision SP 80 system ( $\pm 3$  mm horizontal,  $\pm 3.5$  mm vertical RMSE)<sup>75,83</sup>. All surveys were conducted with a DJI Phantom 4 Pro, which carries a 1" CMOS sensor camera, with the exception of the site 1 2022 survey, which was conducted with a DJI Matrice 600 Pro mounted with a Ronin-MX carrying a Sony a7ii camera. Flight plans were created using the DJI Ground Station Pro app. All flights were conducted using the same settings for comparisons across sites (Supplementary Table 9).

Following the sUAS and RTK-GNSS surveys, we discarded poorly focused images, and processed the remaining images using Structure-from Motion (SfM) photogrammetry. This technique aligns overlapping images by matching common features to create tie points, generating detailed DEMs. GCPs were used to georeference the SfM products to NAD83(2011), UTM Zone 18 N (EPSG:6318), with elevations referenced to NAVD88 using the Geoid 18 model. A quality control assessment was conducted on the image network to identify and correct errors, ensuring the reliability of the tie points<sup>76,77</sup>. To assess georeferencing accuracy, Monte Carlo simulations were employed by randomly selecting GCPs to assess the xyz error of each georeferenced image network<sup>78,79</sup>. The refined image network was used to generate high-resolution ( $\leq 1$  cm) and vertically accurate (RMSE  $\leq 3$  cm) DEMs.

DEMs were used to quantify structural features, including crest elevation, base elevation, and total height (crest minus base). Breakwater base width measurements extracted from DEMs were validated against in situ observations collected from the Trimble R10 RTK-GNSS receiver.

### Comparison to Goda and Ahrens (2008) breakwater transmission model

We selected the Goda and Ahrens<sup>55</sup> breakwater transmission model as the most appropriate model for our experimental setup, based on a literature review and equation testing. The following criteria were used to evaluate candidate formulae:

1. The breakwater structure must be intertidal—not fully submerged or emergent.
2. The formula must include a nominal diameter or effective structural scale as a parameter.
3. The study must be published in English.

Three studies met these criteria: Ahrens<sup>56</sup>, Goda and Ahrens<sup>55</sup>, and Tomasicchio and Alessandro<sup>80</sup>. Among these, Goda and Ahrens<sup>55</sup> was selected for application after testing revealed it produced the best fit (highest  $R^2$ ) with our observed wave transmission data.

We applied the Goda and Ahrens<sup>55</sup> formulation to all four wave gauge datasets (Site 1 and Site 2 in both 2022 and 2024) to assess how accurately the equation could predict measured transmission coefficients.

When the structure is submerged, transmission occurs over the reef in Zone 1 (relative freeboard  $F/H_I < 0$ ) following Eq. (1) (Tanaka 1976, translated by Goda and Ahrens<sup>55</sup>. When the structure is emergent, transmission occurs over the reef in Zone 3 (relative freeboard  $F/H_I > 0$ ) following Eq. (2) (Numata 1975, translated by Goda and Ahrens<sup>55</sup>.

The concept of energy summation is applied to produce a model that encompasses zones of relative freeboard where the structure is submerged (Zone 1), emergent (Zone 3), and the transition zone (Zone 2) where crests are barely exposed and transmission occurs as a combination of transmission through pore spaces and by wave runup and overtopping<sup>55,81</sup>:

$$K_{T\text{all}} = \min \left\{ 1.0, \sqrt{K_{T\text{over}}^2 + K_h^2 K_{T\text{thru}}^2} \right\} \quad \text{where } K_h = \min \left\{ 1.0, \frac{h_{\text{crest}}}{h + H_I} \right\} \quad (9)$$

$B_{\text{eff, over}}$  is represented as  $(9 * \text{crest width} + \text{bottom width})/10$  while  $B_{\text{eff, thru}}$  is represented as the bottom width. For comprehensive details on equation application and formulation please see Goda and Ahrens<sup>55</sup>.

### Parameter optimization for transmission coefficient modeling

To determine the optimal values of  $D_{eff, over}$  and  $D_{eff, thru}$  that maximize model fit, an iterative parameter search was performed. A range of candidate values for  $D_{eff, over}$  and  $D_{eff, thru}$  was generated, and for each combination,  $K_{Tall}$  was generated. The coefficient of determination ( $R^2$ ) was calculated for each iteration by comparing predicted and observed transmission coefficients. The optimal parameter set was selected as the combination that maximized  $R^2$ .

### Relating effective diameter to oyster parameters

Collected oyster parameters at both sites and years were averaged by site and year, yielding for mean oyster lengths, percent gap coverages, and oyster densities. To determine the potential influence of oyster parameters on  $D_{eff, over}$  and  $D_{eff, thru}$ , and thus wave transmission, a Bayesian linear regression model was fitted for each year and site. Bayesian regression was chosen due to the small sample size ( $n = 4$ ), enabling probabilistic estimates and uncertainty quantification. Models were implemented in MATLAB using the `bayeslm` function with `ModelType = 'diffuse'`, which applies a flat prior on the regression coefficients and an improper Jeffreys prior on the error variance<sup>71</sup>. The posterior distribution was computed analytically, without the use of Markov chain Monte Carlo (MCMC) sampling. A diffuse (or weakly informative) prior was chosen to allow the data to dominate inference. This approach was chosen because prior knowledge on the relationship between oyster parameters and effective diameter was limited, and our goal was to avoid unduly constraining model outcomes, especially given our small sample size<sup>82</sup>. The diffuse prior ensured that the posterior distributions reflected information primarily from the data rather than from strong prior assumptions. The covariates tested included mean oyster length on reef surfaces (cm), mean oyster length in gaps (cm), percent gap coverage (%), and oyster density (oysters/m<sup>2</sup>), each modeled separately to evaluate their relationship with effective diameter.

Model fit was evaluated using multiple approaches to assess the reliability and predictive performance of the models. Posterior credible intervals were examined to quantify parameter uncertainty and determine whether the estimated regression coefficients provided strong evidence for a relationship between the oyster predictors and  $D_{eff, over}$  or  $D_{eff, thru}$ . Residual analysis was conducted to identify potential patterns in model errors. While most models showed no systematic trends or heteroscedasticity, two models (surface and gap oyster length vs.  $D_{eff, thru}$ ) exhibited a modest increase in residual spread with higher fitted values, which may suggest heteroscedasticity (Supplementary Fig. 4). Given the limited sample size ( $n = 4$ ), we retained the linear form while acknowledging this limitation. Posterior predictive checks were performed to compare observed and predicted values, providing insight into how well the models captured the variability in the data. Finally, a comparison between predictors was undertaken to assess which oyster predictor most effectively explained variations in  $D_{eff, over}$  and  $D_{eff, thru}$ .

### Data availability

The datasets generated during and/or analyzed during the current study are via figshare: [<https://figshare.com/s/bf8ce9a37d2a22c0a5cc>](<https://figshare.com/s/bf8ce9a37d2a22c0a5cc>).

Received: 23 July 2025; Accepted: 17 November 2025

Published online: 29 November 2025

### References

1. Neumann, B., Vafeidis, A. T., Zimmermann, J. & Nicholls, R. J. Future coastal population growth and exposure to Sea-Level rise and coastal Flooding - A global assessment. *PLoS ONE*. **10**, e0118571 (2015).
2. Intergovernmental Panel On Climate Change (IPCC). *Climate Change 2022 – Impacts, Adaptation and Vulnerability: Working Group II Contribution To the Sixth Assessment Report of the Intergovernmental Panel on Climate Change* <https://doi.org/10.1017/9781009325844> (Cambridge University Press, 2023).
3. Arkema, K. K. et al. Coastal habitats shield people and property from sea-level rise and storms. *Nat. Clim. Change*. **3**, 913–918 (2013).
4. Magnan, A. K. et al. Sea level rise risks and societal adaptation benefits in low-lying coastal areas. *Sci. Rep.* **12**, 10677 (2022).
5. Gittman, R. K., Scyphers, S. B., Smith, C. S., Neylan, I. P. & Grabowski, J. H. Ecological consequences of shoreline hardening: a meta-analysis. *BioScience* **66**, 763–773 (2016).
6. Gracia, A., Rangel-Buitrago, N., Oakley, J. A. & Williams, A. T. Use of ecosystems in coastal erosion management. *Ocean. Coast. Manag.* **156**, 277–289 (2018).
7. Rangel-Buitrago, N., Williams, A. T. & Anfuso, G. Hard protection structures as a principal Coastal erosion management strategy along the Caribbean Coast of Colombia. A chronicle of pitfalls. *Ocean. Coast. Manag.* **156**, 58–75 (2018).
8. Barbier, E. B. et al. The value of estuarine and coastal ecosystem services. *Ecol. Monogr.* **81**, 169–193 (2011).
9. Floerl, O. et al. A global model to forecast coastal hardening and mitigate associated socioecological risks. *Nat. Sustain.* **4**, 1060–1067 (2021).
10. Gittman, R. K. et al. Engineering away our natural defenses: an analysis of shoreline hardening in the US. *Front. Ecol. Environ.* **13**, 301–307 (2015).
11. Lam, N. W. Y., Huang, R. & Chan, B. K. K. Variations in intertidal assemblages and zonation patterns between vertical artificial seawalls and natural Rocky shores: A case study from Victoria Harbour, Hong Kong. *Zool. Stud.* **48**, 184–195 (2009).
12. Gittman, R. K., Popowich, A. M., Bruno, J. F. & Peterson, C. H. Marshes with and without sills protect estuarine shorelines from erosion better than bulkheads during a category 1 hurricane. *Ocean. Coast. Manag.* **102**, 94–102 (2014).
13. Narayan, S. et al. The effectiveness, costs and coastal protection benefits of natural and nature-based defences. *PLoS ONE*. **11**, e0154735 (2016).
14. Feagin, R. A. et al. Infrastructure investment must incorporate nature's lessons in a rapidly changing world. *One Earth*. **4**, 1361–1364 (2021).
15. Bridges, T. S. et al. *Use of Natural and Nature-Based Features (NNBF) for Coastal Resilience*. ERDC SR-15-1. <https://usace.contentdm.oclc.org/digital/collection/p266001coll1/id/3442/> (U.S. Army Engineer Research and Development Center, 2015).

16. U.S. Army Corps of Engineers. Coastal risk reduction and resilience: using the full array of measures. [https://ewn.ercd.dren.mil/wp-content/uploads/2021/02/2\\_USACE\\_CW-Coastal\\_Risk\\_Reduction\\_and\\_Resilience\\_Reduced.pdf](https://ewn.ercd.dren.mil/wp-content/uploads/2021/02/2_USACE_CW-Coastal_Risk_Reduction_and_Resilience_Reduced.pdf) (US Army Corps of Engineers, Civil Works Directorate, 2013).
17. Morris, R. L. et al. Large-scale variation in wave Attenuation of oyster reef living shorelines and the influence of inundation duration. *Ecol. Appl.* **31**, e02382 (2021).
18. Wiberg, P. L., Taube, S. R., Ferguson, A. E., Kremer, M. R. & Reidenbach, M. A. Wave Attenuation by oyster reefs in shallow coastal Bays. *Estuaries Coasts.* **42**, 331–347 (2019).
19. Hogan, S., Wiberg, P. & Reidenbach, M. Utilizing airborne lidar data to quantify marsh edge morphology and the role of oyster reefs in mitigating marsh erosion. *Mar. Ecol. Prog Ser.* **669**, 17–31 (2021).
20. Chowdhury, M. S. N., Hossain, M. S., Ysebaert, T. & Smaal, A. C. Do oyster breakwater reefs facilitate benthic and fish fauna in a dynamic subtropical environment? *Ecol. Eng.* **142**, 105635 (2020).
21. Silva, R., Mendoza, E., Mariño-Tapia, I., Martínez, M. L. & Escalante, E. An artificial reef improves coastal protection and provides a base for coral recovery. *J. Coast Res.* **75**, 467–471 (2016).
22. Higgins, E., Metaxas, A. & Scheibling, R. E. A systematic review of artificial reefs as platforms for coral reef research and conservation. *PLoS ONE.* **17**, e0261964 (2022).
23. McAfee, D., McLeod, I. M., Boström-Einarsson, L. & Gillies, C. L. The value and opportunity of restoring australia's lost rock oyster reefs. *Restor. Ecol.* **28**, 304–314 (2020).
24. Walles, B. et al. From artificial structures to self-sustaining oyster reefs. *J. Sea Res.* **108**, 1–9 (2016).
25. Goelz, T., Vogt, B. & Hartley, T. Alternative substrates used for oyster reef restoration: A review. *J. Shellfish Res.* **39**, 1 (2020).
26. Lipcius, R. N. & Burke, R. P. Successful recruitment, survival and long-term persistence of Eastern oyster and hooked mussel on a subtidal, artificial restoration reef system in Chesapeake Bay. *PLoS ONE.* **13**, e0204329 (2018).
27. Rodriguez, A. B. et al. Oyster reefs can outpace sea-level rise. *Nat. Clim. Change.* **4**, 493–497 (2014).
28. Ridge, J. T. et al. Maximizing oyster-reef growth supports green infrastructure with accelerating sea-level rise. *Sci. Rep.* **5**, 14785 (2015).
29. Hogan, S. & Reidenbach, M. A. Quantifying tradeoffs in ecosystem services under various oyster reef restoration designs. *Estuaries Coasts.* **45**, 677–690 (2022).
30. Wen, C. K. C., Pratchett, M. S., Almany, G. R. & Jones, G. P. Patterns of recruitment and microhabitat associations for three predatory coral reef fishes on the Southern great barrier Reef, Australia. *Coral Reefs.* **32**, 389–398 (2013).
31. Schotanus, J. et al. Restoring mussel beds in highly dynamic environments by Lowering environmental stressors. *Restor. Ecol.* **28**, 1124–1134 (2020).
32. Wakefield, S. Making nature into infrastructure: the construction of oysters as a risk management solution in new York City. *Environ. Plan. E Nat. Space.* **3**, 761–785 (2020).
33. Fivash, G. S. et al. Can we enhance ecosystem-based coastal defense by connecting oysters to marsh edges? Analyzing the limits of oyster reef establishment. *Ecol. Eng.* **165**, 106221 (2021).
34. Wang, X. et al. Structural and functional improvements of coastal ecosystem based on artificial oyster reef construction in the Bohai Sea, China. *Front. Mar. Sci.* **9**, 829557 (2022).
35. Wheaton, F. Review of the properties of Eastern oysters, *Crassostrea virginica*. *Aquacult. Eng.* **37**, 3–13 (2007).
36. Styles, R. Flow and turbulence over an oyster reef. *J. Coast Res.* **314**, 978–985 (2015).
37. Reidenbach, M. A., Berg, P., Hume, A., Hansen, J. C. R. & Whitman, E. R. Hydrodynamics of intertidal oyster reefs: the influence of boundary layer flow processes on sediment and oxygen exchange. *Limnol. Oceanogr. Fluids Environ.* **3**, 225–239 (2013).
38. Coen, L. D., Luckenbach, M. W. & Breitburg, D. L. The role of oyster reefs as essential fish habitat: A review of current knowledge and some new perspectives. In *Fish Habitat: Essential Fish Habitat and Rehabilitation*, 438–454. <https://doi.org/10.47886/9781888569124> (American Fisheries Society, 1999).
39. Wu, F., Yin, Z., Gao, C., Feng, H. & Wang, Y. Hydrodynamics of oyster reefs: A systematic review. *Ocean. Eng.* **311**, 118954 (2024).
40. Bayne, B. L. *Biology of Oysters* (Elsevier Science, 2017).
41. Cannon, D. J., Kibler, K. M., Taye, J. & Medeiros, S. C. Characterizing canopy complexity of natural and restored intertidal oyster reefs (*Crassostrea virginica*) with a novel laser-scanning method. *Restor. Ecol.* **31**, e13973 (2023).
42. Kitsikoudis, V., Kibler, K. M. & Walters, L. J. In-situ measurements of turbulent flow over intertidal natural and degraded oyster reefs in an estuarine lagoon. *Ecol. Eng.* **143**, 105688 (2020).
43. Cannon, D., Kibler, K. M., Kitsikoudis, V., Medeiros, S. C. & Walters, L. J. Variation of mean flow and turbulence characteristics within canopies of restored intertidal oyster reefs as a function of restoration age. *Ecol. Eng.* **180**, 106678 (2022).
44. Ribas-Deulofeu, L., Château, P. A., Denis, V. & Chen, C. A. Portraying gradients of structural complexity in coral reefs using Fine-Scale depth profiles. *Front. Mar. Sci.* **8**, 675853 (2021).
45. Mathews, H., Uddin, M. J., Hargis, C. W. & Smith, K. J. First-Year performance of the pervious oyster shell habitat (POSH) along two energetic shorelines in Northeast Florida. *Sustainability* **15**, 7028 (2023).
46. Webb, B. M. & Allen, R. Wave Transmission Through Artificial Reef Breakwaters. in *Coastal structures and solutions to coastal disasters 2015*, 432–444. American Society of Civil Engineers, Boston, Massachusetts, United States <https://doi.org/10.1061/9780784480304.046> (2017).
47. Dunlop, T., Felder, S., Glamore, W. C., Howe, D. & Coghlan, I. R. Optimising ecological and engineering values in coastal protection via combined oyster shell and sand bag designs. In *Australasian Coasts & Ports 2017: Working with Nature, Coasts and Ports Conference* (2017).
48. Xu, W. et al. Experimental investigation on wave Attenuation of oyster castles in optimized layout based on Bragg resonance. *Ocean. Eng.* **321**, 120426 (2025).
49. Chauvin, J. *Wave attenuation by constructed oyster reef breakwaters*. MSc thesis, Louisiana State University and Agricultural and Mechanical College. [https://doi.org/10.31390/gradschool\\_theses.4752](https://doi.org/10.31390/gradschool_theses.4752) (2018).
50. Spiering, D. W., Kibler, K. M., Kitsikoudis, V., Donnelly, M. J. & Walters, L. J. Detecting hydrodynamic changes after living shoreline restoration and through an extreme event using a Before-After-Control-Impact experiment. *Ecol. Eng.* **169**, 106306 (2021).
51. Bredes, A. L., Miller, J. K., Kerr, L. & Brown, D. R. Observations of wave height amplification behind an oyster castle breakwater system in a High-Energy environment: Gandys Beach, NJ. *Front. Built Environ.* **8**, 884795 (2022).
52. Manis, J. E., Garvis, S. K., Jachec, S. M. & Walters, L. J. Wave Attenuation experiments over living shorelines over time: a wave tank study to assess recreational boating pressures. *J. Coast Conserv.* **19**, 1–11 (2015).
53. Kim, M., Jung, S., Chau, T. V. & Na, W. B. Correlation of the structural characteristics of an artificial oyster reef with its wake region. *J. Mar. Sci. Eng.* **11**, 775 (2023).
54. Srineash, V. K. & Murali, K. Functional performance of modular porous reef breakwaters. *J. Hydro Environ. Res.* **27**, 20–31 (2019).
55. Goda, Y. & Ahrens, J. P. New formulation of wave transmission over and through low-crested structures. In *Coastal Engineering Proceedings of the 31st International Conference* 3530–3541. [https://doi.org/10.1142/9789814277426\\_0293](https://doi.org/10.1142/9789814277426_0293) (World Scientific, 2008).
56. Ahrens, J. P. & United States. *Characteristics of Reef Breakwaters*. Technical Report CERC-87-17. U.S. Army Corps of Engineers, Waterways Experiment Station, Vicksburg, Mississippi. <https://www.ancientportsantiques.com/wp-content/uploads/Documents/ENGINEERING/Maritime/BW/ReefBW-Ahrens1987.pdf> (1987).
57. Fodrie, F. J. et al. Classic paradigms in a novel environment: inserting food web and productivity lessons from Rocky Shores and saltmarshes into biogenic reef restoration. *J. Appl. Ecol.* **51**, 1314–1325 (2014).

58. Robinson, E., Lunt, J., Marshall, C. & Smee, D. Eastern oysters *Crassostrea Virginica* deter crab predators by altering their morphology in response to crab cues. *Aquat. Biol.* **20**, 111–118 (2014).
59. Ziegler, S. L., Grabowski, J. H., Baillie, C. J. & Fodrie, F. J. Effects of landscape setting on oyster reef structure and function largely persist more than a decade post-restoration. *Restor. Ecol.* **26**, 933–942 (2018).
60. Menge, B. A. & Sutherland, J. P. Community regulation: variation in Disturbance, Competition, and predation in relation to environmental stress and recruitment. *Am. Nat.* **130**, 730–757 (1987).
61. Denny, M. W., Daniel, T. L. & Koehl, M. A. R. Mechanical limits to size in Wave-Swept organisms. *Ecol. Monogr.* **55**, 69–102 (1985).
62. Grabowski, J. H. Habitat complexity disrupts Predator–Prey interactions cut not the trophic cascade on oyster reefs. *Ecology* **85**, 995–1004 (2004).
63. Kurdistani, S. M., Tomasicchio, G. R., D’Alessandro, F. & Francone, A. Formula for wave transmission at submerged homogeneous porous breakwaters. *Ocean. Eng.* **266**, 113053 (2022).
64. Goda, Y. *Random Seas and Design of Maritime Structures* **33** (World Scientific, 2010).
65. Gittman, R. K. et al. Living shorelines can enhance the nursery role of threatened estuarine habitats. *Ecol. Appl.* **26**, 249–263 (2016).
66. Moore, C. S., Gittman, R. K., Puckett, B. J., Wellman, E. H. & Blakeslee, A. M. H. If you build it, they will come: restoration positively influences free-living and parasite diversity in a restored tidal marsh. *Food Webs.* **25**, e00167 (2020).
67. Trimble Inc. Trimble R10 Model 2 GNSS System Datasheet. <https://www.laserinst.com/content/Datasheet%20-%20Trimble%20R10%20Model%202%20-%20English%20%28USL%29%20-%20Screen.pdf> (2018).
68. Temple, N. A., Webb, B. M., Sparks, E. L. & Linhoss, A. C. Low-Cost pressure gauges for measuring water waves. *J. Coast Res.* **36**, 661 (2020).
69. NOAA National Data Buoy Center (NDBC). Station BFTN7 – Beaufort, NC (Data). National Oceanic and Atmospheric Administration. [https://www.ndbc.noaa.gov/station\\_page.php?station=bftn7](https://www.ndbc.noaa.gov/station_page.php?station=bftn7).
70. Denny, M. W. *Biology and the Mechanics of the Wave-Swept Environment* (Princeton University Press, 1988).
71. MATLAB. Version R. (MathWorks, Natick, MA, 2024).
72. Karimpour, A. & Chen, Q. Wind wave analysis in depth limited water using OCEANLYZ, A MATLAB toolbox. *Comput. Geosci.* **106**, 181–189 (2017).
73. R Core Team. *R: A Language and Environment for Statistical Computing* (R Foundation for Statistical Computing, 2024).
74. Scrucca, L. Model-based SIR for dimension reduction. *Comput. Stat. Data Anal.* **55**, 3010–3026 (2011).
75. Trimble & Trimble Inc. *SP80 GNSS Receiver User Guide..* <https://trl.trimble.com/docushare/dsweb/Get/Document-844535/SG-SP80-Br-v2.pdf> (2019).
76. James, M. R., Robson, S., d’Oleire-Oltmanns, S. & Niethammer, U. Optimising UAV topographic surveys processed with structure-from-motion: ground control quality, quantity and bundle adjustment. *Geomorphology* **280**, 51–66 (2017).
77. Cooper, H. M. et al. Evaluating the ability of Multi-Sensor techniques to capture topographic complexity. *Sensors* **21**, 2105 (2021).
78. James, M. R., Robson, S. & Smith, M. W. 3-D uncertainty-based topographic change detection with structure-from-motion photogrammetry: precision maps for ground control and directly georeferenced surveys. *Earth Surf. Process. Landf.* **42**, 1769–1788 (2017).
79. Guan, S., Sirianni, H., Wang, G. & Zhu, Z. sUAS monitoring of coastal environments: A review of best practices from field to lab. *Drones* **6**, 142 (2022).
80. Tomasicchio, G. R. & D’Alessandro, F. Wave energy transmission through and over low crested breakwaters. *J. Coastal. Res.* **65**, 398–403 (2013).
81. Wamsley, T. V. & Ahrens, J. P. Computation of wave transmission coefficients at detached breakwaters for shoreline response modeling. In *Coastal Structures 2003*, 593–605. [https://doi.org/10.1061/40733\(147\)49](https://doi.org/10.1061/40733(147)49) (American Society of Civil Engineers, 2004).
82. Gelman, A., Jakulin, A., Pittau, M. G. & Su, Y. S. A weakly informative default prior distribution for logistic and other regression models. *Ann. Appl. Stat.* **2**, (2008).
83. Megan E., Geesin Georgette L., Tso Hannah, Sirianni Siddharth, Narayan Chris J., Baillie Praveen D., Malali Brandon J., Puckett Justin T., Ridge Rachel K., Gittman (2025) Assessing the effects of engineered oyster reefs on shoreline change using drones. *Frontiers in Ecology and Evolution* <https://doi.org/1310.3389/fevo.2025.1616227>

## Author contributions

GLT, RKG, and SN conceived and designed the study. GLT, RKG, and MEG conducted the field experiments and collected the necessary data. GLT and SN analyzed the data. GLT, RKG, SN, MEG, HS, JF, MAR wrote the manuscript and prepared the figures. All authors reviewed the manuscript and approved the final version.

## Funding

This work was supported by the National Oceanic and Atmospheric Administration (NOAA) through the U.S. Coastal Research Program (USCRP) and the National Sea Grant College Program (Grant ID: NA23OAR4170122). Additional support was provided by the North Carolina Sea Grant (Grant IDs: 2011-1590-10 R/NCSG-RM-22-03 and NA18OAR4170069, Subaward 2018-2791-18; R/MG-2203) and the National Science Foundation (Grant IDs: 2206479 and DGE-2125684). The funding agencies had no role in the design of the study, data collection and analysis, decision to publish, or preparation of the manuscript. Data and information presented in this study has not formally been disseminated by the funding agencies and do not represent any agency determination, view, or policy.

## Declarations

### Competing interests

The authors declare no competing interests.

### Additional information

**Supplementary Information** The online version contains supplementary material available at <https://doi.org/10.1038/s41598-025-29349-9>.

**Correspondence** and requests for materials should be addressed to G.L.T.

**Reprints and permissions information** is available at [www.nature.com/reprints](http://www.nature.com/reprints).

**Publisher's note** Springer Nature remains neutral with regard to jurisdictional claims in published maps and institutional affiliations.

**Open Access** This article is licensed under a Creative Commons Attribution-NonCommercial-NoDerivatives 4.0 International License, which permits any non-commercial use, sharing, distribution and reproduction in any medium or format, as long as you give appropriate credit to the original author(s) and the source, provide a link to the Creative Commons licence, and indicate if you modified the licensed material. You do not have permission under this licence to share adapted material derived from this article or parts of it. The images or other third party material in this article are included in the article's Creative Commons licence, unless indicated otherwise in a credit line to the material. If material is not included in the article's Creative Commons licence and your intended use is not permitted by statutory regulation or exceeds the permitted use, you will need to obtain permission directly from the copyright holder. To view a copy of this licence, visit <http://creativecommons.org/licenses/by-nc-nd/4.0/>.

© The Author(s) 2025